Nitrogen Photofixation

International Edition: DOI: 10.1002/anie.201511189
German Edition: DOI: 10.1002/ange.201511189

Selective Dinitrogen Conversion to Ammonia Using Water and Visible Light through Plasmon-induced Charge Separation

*Tomoya Oshikiri, Kosei Ueno, and Hiroaki Misawa**

Abstract: *The generation of ammonia from atmospheric nitrogen and water using sunlight is a preferable approach to obtaining ammonia as an energy carrier and potentially represents a new paradigm for achieving a low-carbon and sustainable-energy society. Herein, we report the selective conversion of dinitrogen into ammonia through plasmon-induced charge separation by using a strontium titanate ($SrTiO_3$) photoelectrode loaded with gold nanoparticles (Au-NPs) and a zirconium/zirconium oxide (Zr/ZrO_x) thin film. We observed the simultaneous stoichiometric production of ammonia and oxygen from nitrogen and water under visible-light irradiation.*

Ammonia has received much attention as a potential energy carrier and as a fuel for vehicles, in addition to its use as a fertilizer[1] because it is a non-carbon-based chemical that is easily condensed into a liquid. Ammonia is conventionally synthesized through the Haber-Bosch process under high energy consumption conditions.[2] Over 90% of the energy consumed by hydrogen production during ammonia synthesis comes from fossil fuels. Therefore, the development of a new process for synthesizing ammonia without the use of hydrogen gas is needed. The generation of ammonia from atmospheric nitrogen and water using sunlight is one of the preferred approaches to synthesizing ammonia as an energy carrier, and potentially represents a new paradigm for a low-carbon and sustainable-energy society. Although there are several reports about nitrogen photoelectrochemical conversion into ammonia, nitrogen photofixation devices that can harvest visible light exhibit low activity and require a sacrificial electron donor.[3] Herein, we report the selective conversion of dinitrogen into ammonia through plasmon-induced charge separation by using a $SrTiO_3$ photoelectrode loaded with gold nanoparticles (Au-NPs) and a Zr thin film. We observed the simultaneous stoichiometric production of ammonia and oxygen from nitrogen and water under visible-light irradiation.

[*] Dr. T. Oshikiri, Prof. K. Ueno, Prof. H. Misawa
Research Institute for Electronic Science
Hokkaido University N21, W10, CRIS Bldg.
Kita-ku, Sapporo 001-0021 (Japan)
E-mail: misawa@es.hokudai.ac.jp
Homepage: http://misawa.es.hokudai.ac.jp/index_en.html
Prof. H. Misawa
Department of Applied Chemistry & Institute of Molecular Science
National Chiao Tung University
1001 Ta Hsueh R., Hsinchu 30010 (Taiwan)

Supporting information for this article can be found under http://dx.doi.org/10.1002/anie.201511189.

The co-catalyst is a critical factor in determining the activity and selectivity of a photocatalytic reaction. Ruthenium (Ru) is widely used as a thermochemical and electrochemical catalyst for nitrogen fixation because of its high activity.[4] However, Ru is also known to adsorb H adatoms more strongly than N adatoms, and thereby become poisoned.[5] Therefore, we focused on the binding affinity of H and N adatoms on the surface of a co-catalyst. Density functional theory calculations on a wide variety of transition-metal surfaces have predicted that the adsorption energy of H (ΔH^*) is smaller than that of N (ΔN^*) on the Ru surface.[6] However, ΔN^* is smaller than ΔH^* on the Zr surface, indicating that it preferentially adsorbs N adatoms. In fact, our electrochemical experiments indicated that a Zr electrode exhibits greater selectivity for NH_3 formation than a Ru electrode (Supporting Information, Figure S1).

Recently, localized surface plasmon resonance (LSPR) of metallic nanostructures has received much attention because of its light-harvesting and electric-field-enhancing effects. These unique properties promote the application of LSPR to many areas, including sensing,[7] photocurrent generation,[8] and photochemical reactions.[9] Previously, we reported a photoelectrochemical reaction using plasmon-induced charge separation.[3c,10] In the present study, we designed an $SrTiO_3$ photoelectrode equipped with Au-NPs as the plasmonic nanostructure and Zr as a co-catalyst. The Au-NPs/niobium-doped strontium titanate (Nb-$SrTiO_3$)/Zr photoelectrode was fabricated as follows. Au-NPs were fabricated on a 0.05 wt% Nb-$SrTiO_3$ single-crystalline substrate using an annealing method. A Zr thin film was then deposited using the electron-beam evaporation method onto the opposite side of the Nb-$SrTiO_3$ substrate. The average and standard deviation of the Au-NP size were estimated to be 45 nm and 18 nm, respectively, from a scanning electron microscope image (Figure S2). The surface coverage ratio of the Nb-$SrTiO_3$ substrate by Au-NPs was estimated to be 19.7%. The X-ray photoelectron spectrum (XPS) and X-ray reflection (XRR) revealed that the surface of the Zr film deposited onto the $SrTiO_3$ was oxidized by air, and that the thicknesses of the zirconium oxide (ZrO_x) and metal zirconium layers were 2.6 nm and 2.2 nm, respectively (Figures S3, S4). The calculated value of ΔN^* has been reported to be smaller than that of ΔH^*, even on ZrO_x.[11] The scanning transmission electron micrographs of Au-NPs/Nb-$SrTiO_3$ and Nb-$SrTiO_3$/Zr are shown in Figure 1a. The lattice structure of $SrTiO_3$ and the interface between Nb-$SrTiO_3$ and Zr are observed clearly; however, an obvious periodic structure of Zr was not observed. The cross-section of the Zr layer is considered to be oxidized after sample preparation for the scanning transmission electron microscope measurement. An Au-NPs/Nb-

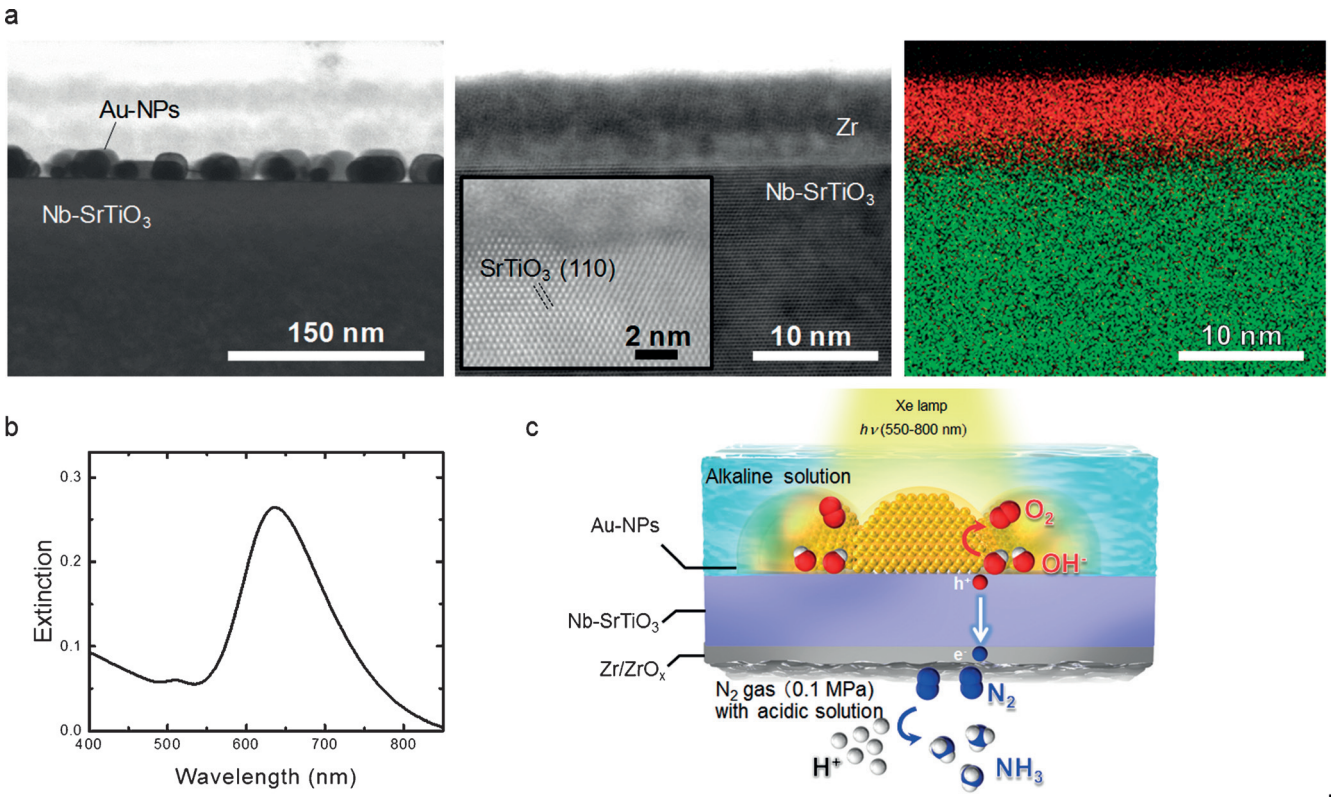

Figure 1. a) Cross-sectional view of the bright-field scanning transmission electron microscopy (BF-STEM) image of the Au-NPs/Nb-$SrTiO_3$ interface (left). Cross-sectional view of the BF-STEM image of the Zr film deposited onto the single-crystalline Nb-$SrTiO_3$ (center; the inset shows the magnified view of the high-angle annular dark-field STEM image) and the corresponding energy-dispersive X-ray spectroscopy (EDS) spectrum. The Zr and Ti signals in the EDS images are indicated by red and green colors, respectively (right). b) Extinction spectrum of the Au-NPs on Nb-$SrTiO_3$. c) Layout of the NH_3 synthesis device bearing the Nb-$SrTiO_3$ photoelectrode loaded with Au-NPs and a Zr/ZrO_x thin film.

$SrTiO_3$/Ru photoelectrode was also prepared in a similar manner as the Au-NPs/Nb-$SrTiO_3$/Zr/ZrO_x electrode.

The extinction spectrum of the Au-NPs on the Nb-$SrTiO_3$ substrate is shown in Figure 1 b. The spectrum clearly shows that the LSPR band exhibited a maximum at approximately 630 nm. The NH_3 synthesis system with an Nb-$SrTiO_3$ substrate loaded with Au-NPs is shown in Figure 1 c. The NH_3 synthesis device contains two compartments for separate collection of the reduction and oxidation products. To promote NH_3 formation, a chemical bias was applied by regulating the pH of these compartments, instead of using an external electrochemical apparatus. The anodic chamber was filled with a potassium hydroxide (KOH) aqueous solution. Simultaneously, an aqueous hydrochloric acid (HCl) solution was injected into the cathodic chamber using N_2 gas. The HCl also serves as a proton source for NH_3 synthesis.

All of the photoelectrochemical experiments were conducted at room temperature. Figure 2 shows an energy diagram for the plasmon-induced NH_3 photosynthesis system with an $SrTiO_3$ photoelectrode loaded with Au-NPs. The principle of this device relies on plasmon-induced charge separation at the Au-NPs/Nb-$SrTiO_3$ interface. We hypothesized that an excited electron is transferred to the $SrTiO_3$ conduction band following the Au-NP interband or intraband transition, or that transfer of an $SrTiO_3$ surface-state electron is induced by the plasmo-induced near-field, or by hot

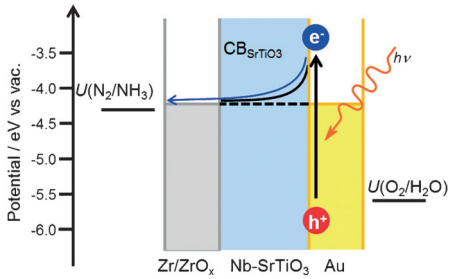

Figure 2. Energy-level diagram of the plasmon-induced NH_3 synthesis device. CB: conduction band; *U*: redox potential.

electron transfer. These events result in holes trapped in the $SrTiO_3$ surface near the Au/Nb-$SrTiO_3$/water interface, and these trapped holes can efficiently induce an oxidation reaction. By contrast, the photogenerated electrons injected into the conduction band of $SrTiO_3$ reduced N_2 at the Zr/ZrO_x surface, which was deposited on the substrate side opposite of the Au-NPs/Nb-$SrTiO_3$. In this way, plasmon-induced NH_3 photosynthesis through nitrogen photofixation was demonstrated.

In the first stage of our work, we investigated the ability of Au-NPs/Nb-$SrTiO_3$/Zr/ZrO_x to form NH_3 with ethanol as a sacrificial electron donor. The pH values of the anode and

cathode solutions were fixed at 13 and 2, respectively. Ethanol (10 vol %) was added to the anodic chamber. The irradiation time dependence of NH_3 formation in the cathodic chamber is shown in Figure 3a. The Au-NPs were irradiated with light

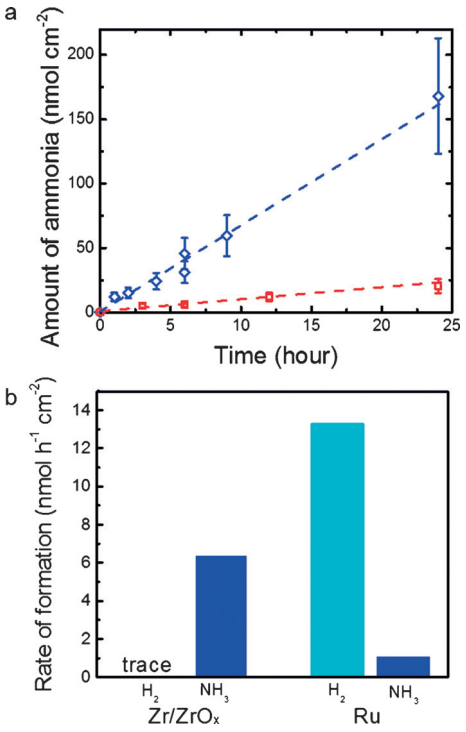

Figure 3. Plasmon-induced NH_3 synthesis using ethanol as a sacrificial electron donor. a) The irradiation time-dependence of NH_3 formation on the cathodic side of the chamber over Au-NPs/Nb-$SrTiO_3$/Zr/ZrO_x (blue diamond) and Au-NPs/Nb-$SrTiO_3$/Ru (red square). The irradiation condition included xenon light spectrally filtered to the wavelengths from 550 nm to 800 nm. b) The reaction rate of each product in the cathodic chamber over Au-NPs/Nb-$SrTiO_3$/Zr/ZrO_x and Au-NPs/Nb-$SrTiO_3$/Ru.

from a xenon lamp, where the light was spectrally filtered to wavelengths from 550 to 800 nm, to excite the LSPR. The amount of NH_3 formed under irradiation of the Nb-$SrTiO_3$ loaded with Au-NPs linearly increased with increasing irradiation time, and the rate of NH_3 formation was 6.5 nmol h^{-1} cm^{-2}. This rate is more than 6-times greater than that in the case where Ru was used as a co-catalyst (1.1 nmol h^{-1} cm^{-2}). Figure 3b indicates the production selectivity for Zr/ZrO_x and Ru. In the case of Au-NPs/Nb-$SrTiO_3$/Ru, the production rate of H_2 was 15-times greater than that of NH_3. This result indicates that proton reduction is the main reaction on the Ru co-catalyst. However, in the case of Au-NPs/Nb-$SrTiO_3$/Zr/ZrO_x, the concentration of evolved H_2 was smaller than the limit of quantitation (4.7×10^{-5} mol dm^{-3}), and NH_3 was the main product. These results indicate that Zr/ZrO_x on the Nb-$SrTiO_3$ exhibits high selectivity and efficiency for NH_3 synthesis. The high reactivity is likely attributable to the adsorbed species on the co-catalyst. Because Zr and ZrO_x are expected to bind N adatoms more strongly than H adatoms,[6a,11a] a large amount of NH_3 is produced compared to the amount of produced H_2. Protons in the solutions are considered to be directly added to an adsorbed N on the Zr/ZrO_x surface. A mixture gas of N_2 and H_2 (v/v = 1:1) was used instead of pure N_2 gas to confirm the effect of H_2 on the reaction over Au-NPs/Nb-$SrTiO_3$/Zr/ZrO_x and Au-NPs/Nb-$SrTiO_3$/Ru. The formation of NH_3 on Ru on the Nb-$SrTiO_3$ was significantly enhanced in the presence of H_2 (1.1 to 6.2 nmol h^{-1} cm^{-2}; Figure S5), whereas NH_3 formation on Zr/ZrO_x on the Nb-$SrTiO_3$ exhibited similar or slightly lower activity (6.4 to 4.3 nmol h^{-1} cm^{-2}). The positive effect of H_2 to NH_3 synthesis on Ru is considered to be high catalytic ability synthesizing NH_3 from N_2 and H_2 gases.[4a] However, the negative effect of the mixture gas of H_2 and N_2 indicate that H_2 is not the main reactant with nitrogen on Zr/ZrO_x. This result supports our hypothesis that the N_2 adsorbed onto Zr/ZrO_x on the Nb-$SrTiO_3$ substrate reacts with protons in the solution rather than with H adatoms.

We subsequently attempted plasmon-induced NH_3 synthesis from N_2 and water by using Au-NPs/Nb-$SrTiO_3$/Zr/ZrO_x without any sacrificial donor. As a result, the formation of both NH_3 and O_2 increased linearly with increasing irradiation time, and the production ratio between NH_3 and O_2 was approximately 4:3 ($NH_3/O_2 = 1.33$; Figure 4a). The rate of NH_3 and O_2 formation was 0.73 nmol h^{-1} cm^{-2} and 0.53 nmol h^{-1} cm^{-2}, respectively. The rate of formation decreased to one-ninth of the rate when ethanol was used as a sacrificial donor. This result indicates that N_2 reduction and water oxidation proceed stoichiometrically. Previously, we reported that water might be efficiently oxidized by multiple stored holes trapped at the surface states of the semiconductor near the hot site of the plasmon.[10a] Therefore, both the efficient Zr co-catalyst and the Au-NPs are considered to contribute to the complete redox reaction. The oxidized zirconium nanofilm surface is speculated to also possess excellent catalytic activity for nitrogen fixation because the XPS and XRR results suggest that the metal Zr was covered by the oxidized layer. The bar chart in Figure 4b shows the action spectrum for the normalized apparent quantum efficiency of NH_3 formation, $NAQY_{NH_3}$. NH_3 formation is strongly related to the LSPR excitation because the value of $NAQY_{NH_3}$ was highly dependent on the position of the LSPR band (solid line). Additionally, NH_3 formation was observed in all visible wavelength regions, indicating that the plasmon-induced NH_3 synthesis system can efficiently utilize visible light.

We also investigated NH_3 synthesis on Au-NPs/Nb-$SrTiO_3$/Zr/ZrO_x from isotopic N_2 gas to obtain direct evidence of N_2 fixation. The photoelectrochemical reaction was promoted by the use of $^{15,15}N_2$ gas (SI Science Co., Ltd.) instead of $^{14,14}N_2$. The formed NH_3 was collected by distillation of the reaction liquid with KOH solution because the cathodic chamber is acidic, and the reaction product was obtained in the form of NH_4Cl. The collected NH_3 was identified by gas chromatography–mass spectrometry (GC-MS). Figure 4c shows the GC-MS chromatograph of the sample obtained from the reaction solution after 46 h of irradiation time of visible light (wavelength from 550 to 800 nm), and that of a standard NH_3 (2.5 ppm) aqueous solution. A peak derived from $^{15}NH_3$ ($m/z = 18$) was clearly observed at the same

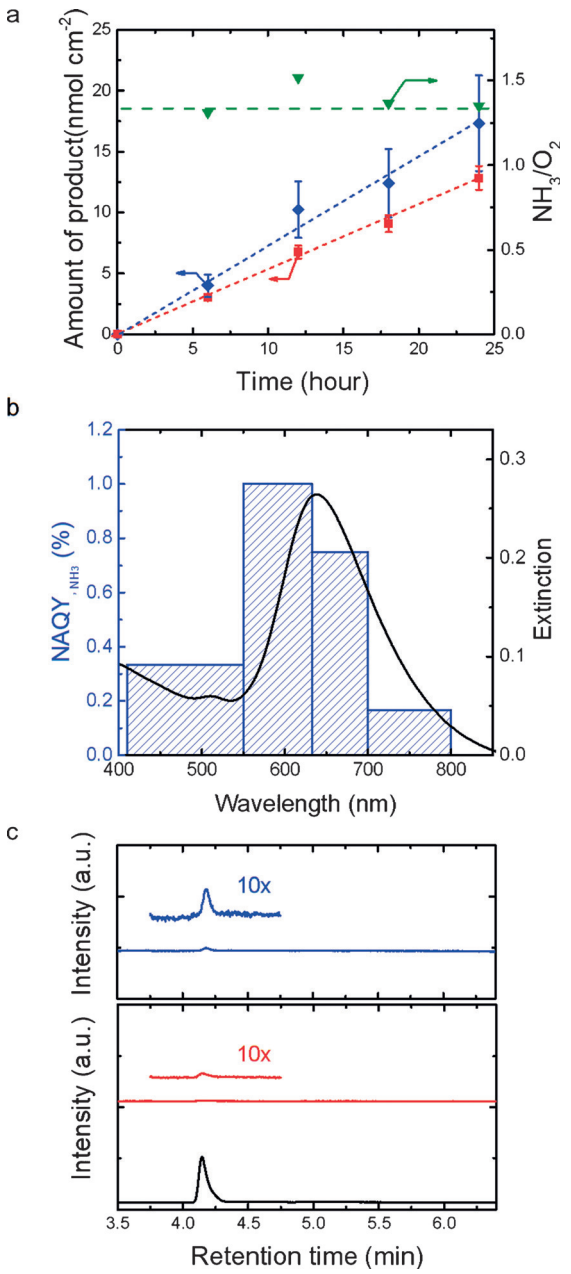

Figure 4. Plasmon-induced NH_3 synthesis on Au-NPs/Nb-$SrTiO_3$/Zr/ZrO_x by using water as an electron donor. a) The irradiation time-dependence of NH_3 formation on the cathodic side of the chamber (blue diamond), O_2 evolution on the anodic chamber (red square), and ratio of NH_3 and O_2 (green triangle), respectively. The dashed green line indicates the ideal stoichiometric ratio (1.33). The irradiation condition included xenon light spectrally filtered to the wavelengths from 550 to 800 nm. b) Histogram of the action spectrum of the normalized apparent quantum efficiency of NH_3 formation for several wavelength regions. The solid line indicates the LSPR band, which is also shown in Figure 1 b. c) GC-MS chromatograph. Upper: sample obtained from the reaction solution after 46 h irradiation time ($m/z = 18$, line in blue). Lower: 2.5 ppm NH_3 aqueous solution ($m/z = 17$, line in black and $m/z = 18$, line in red). The insets show magnified view from 3.75 to 4.75 min.

retention time as a standard $^{14}NH_3$ aqueous solution ($m/z = 17$). Furthermore, the $^{15}NH_3$ peak intensity from the reaction solution was much larger than the natural abundance ratio of ^{15}N. Of course, no obvious peak derived from $^{15}NH_3$ was observed when $^{14,14}N_2$ was used as the reaction gas (Figure S6). These results provide direct evidence that N_2 gas and water were converted into NH_3 under visible-light irradiation.

In conclusion, we report a highly selective and visible-light-responsive plasmonic NH_3 synthesis device containing a Au nanostructure and a Zr/ZrO_x thin film. N_2 gas was reduced to NH_3 using water as an electron donor under visible light irradiation. Although the energy conversion efficiency of this plasmon-induced NH_3 synthesis is still insufficient for practical use, we expect the efficiency will be improved by increasing the reaction surface area and harvesting the proportion of the incident solar energy flux by fabricating the semiconductors as array structures with large surface areas, such as nanotube or nanohole array structures. Understanding of the plasmon-induced charge separation mechanism and control of electron transport are also important for increasing the efficiency of the plasmonic photoelectrochemical reaction. Our system may help the energy infrastructure and security because sunlight-driven NH_3 synthesis is suitable for use in a distributed energy production system.

Experimental Section

Preparation of Au-NPs and Zr film on an $SrTiO_3$ substrate: A single crystal of 0.05 wt% Nb-$SrTiO_3$ ($10 \times 10 \times 0.5$ mm^3, Furuuchi Chemical) with a (110) surface was used as a semiconductor photoelectrode for N_2 fixation. Au-NPs were prepared using the reported procedure.[3c] A thin Zr film was deposited on the opposite side of the Nb-$SrTiO_3$ substrate through electron-beam deposition (ED-1500R, SUNVAC) at a deposition rate of 0.05 $nm\,s^{-1}$. The morphology of Au-NPs on the Nb-$SrTiO_3$ was observed using field-emission scanning electron microscopy (FE-SEM, JSM-6700FT, JEOL). The maximum resolution attainable at an electron acceleration voltage of 15 kV was 1 nm. The cross-sectional structures of the Au-NPs/Nb-$SrTiO_3$ and Zr/Nb-$SrTiO_3$ interfaces were observed by energy-dispersive X-ray spectroscopy (EDS) and scanning transmission electron microscopy (STEM) performed on a JEOL JEM-ARM 200F operated at 200 kV with aberration correction or a Hitachi HD-2000 operated at 200 kV. The cross-sectional STEM samples were prepared using the focused ion beam technique (JEOL JIB-4600F/HKD) with Ga ions accelerated at a voltage of 30 kV.

Photoelectrochemical reaction: The Au-nanostructured Nb-$SrTiO_3$ substrate was irradiated in an area of $\varphi 6$ mm by a xenon lamp using an arbitrary light intensity and wavelength, and the amount of NH_3 formed per area was calculated by dividing the value by the irradiation area. The apparent quantum yield (AQY, %) of the NH_3 formation system, in which three photons are theoretically required to produce one NH_3 molecule, was determined using Equation (1):

$$AQY_{NH_3} = \frac{[\text{Reaction rate of } NH_3 \text{ formation } (\text{mol s}^{-1})] \times 3}{[\text{Incident photon flux } (\text{mol s}^{-1})]} \times 100$$

The incident photon flux was measured using a spectroradiometer (MSR-7000N, Optoresearch) at each wavelength. The AQY_{NH_3} at each wavelength was normalized by dividing the values by the AQY_{NH_3} at 550 to 630 nm ($NAQY_{NH_3}$).

Assays: The quantity of NH_3 formed and evolved O_2 and H_2 were determined using reported methods.[3c] The $^{15}NH_3$ was quantitatively analyzed using GC-MS. See the Supporting Information for full details of the colorimetric quantity of NH_3 and the gas chromatography conditions.

Acknowledgements

We are grateful to Ms. Yuko Mori and Ms. Naomi Kawai at Hokkaido University for STEM measurements. This study was supported by funding from the Ministry of Education, Culture, Sports, Science, and Technology of Japan: KAKENHI Grant-in-Aid for Scientific Research(S) (no. 23225006), Grant-in-Aid for young Scientist (B) (no. 15K17438), and the Innovative Areas "Artificial Photosynthesis (AnApple)" (no. 25107501) grant from the Nanotechnology Platform (Hokkaido University), and the Low-Carbon Research Network of Japan.

Keywords: ammonia · localized surface plasmon · nanostructures · nitrogen fixation · photochemistry

How to cite: *Angew. Chem. Int. Ed.* **2016**, *55*, 3942–3946
Angew. Chem. **2016**, *128*, 4010–4014

[1] a) L. Green, Jr., *Int. J. Hydrogen Energy* **1982**, *7*, 355–359; b) A. Klerke, C. H. Christensen, J. K. Nørskov, T. Vegge, *J. Mater. Chem.* **2008**, *18*, 2304; c) R. Lan, J. T. S. Irvine, S. Tao, *Int. J. Hydrogen Energy* **2012**, *37*, 1482–1494.

[2] a) K. Aika, L. J. Chiristiansen, I. Dybkjacr, J. B. Hansen, H. Nielsen, A. Nielsen, P. Stoltze, K. Tamaru in *Catalysis and Manufacture*, Springer, Heidelberg, **1995**; b) R. Schlögl, *Angew. Chem. Int. Ed.* **2003**, *42*, 2004–2008; *Angew. Chem.* **2003**, *115*, 2050–2055; c) G. Ertl, *Angew. Chem. Int. Ed.* **2008**, *47*, 3524–3535; *Angew. Chem.* **2008**, *120*, 3578–3590.

[3] a) O. Rusina, A. Eremenko, G. Frank, H. P. Strunk, H. Kisch, *Angew. Chem. Int. Ed.* **2001**, *40*, 3993–3995; *Angew. Chem.* **2001**, *113*, 4115–4117; b) O. Rusina, O. Linnik, A. Eremenko, H. Kisch, *Chem. Eur. J.* **2003**, *9*, 561–565; c) T. Oshikiri, K. Ueno, H. Misawa, *Angew. Chem. Int. Ed.* **2014**, *53*, 9802–9805; *Angew. Chem.* **2014**, *126*, 9960–9963.

[4] a) K. Aika, *Angew. Chem. Int. Ed. Engl.* **1986**, *25*, 558–559; *Angew. Chem.* **1986**, *98*, 556–557; b) H. Bielawa, O. Hinrichsen, A. Birkner, M. Muhler, *Angew. Chem. Int. Ed.* **2001**, *40*, 1061–1063; *Angew. Chem.* **2001**, *113*, 1093–1096; c) S.-Y. Zhang, X.-Y. Zhang, Z.-S. Zhang, Y. Kong, S.-N. Hua, *Chem. Lett.* **2003**, *32*, 440–441; d) M. Kitano, Y. Inoue, Y. Yamazaki, F. Hayashi, S. Kanbara, S. Matsuishi, T. Yokoyama, S. W. Kim, M. Hara, H. Hosono, *Nat. Chem.* **2012**, *4*, 934–940.

[5] a) F. Rosowski, A. Hornung, O. Hinrichsen, D. Herein, M. Muhler, G. Ertl, *Appl. Catal. A* **1997**, *151*, 443–460; b) S. Siporin, *J. Catal.* **2004**, *225*, 359–368.

[6] a) E. Skúlason, T. Bligaard, S. Gudmundsdottir, F. Studt, J. Rossmeisl, F. Abild-Pedersen, T. Vegge, H. Jonsson, J. K. Norskov, *Phys. Chem. Chem. Phys.* **2012**, *14*, 1235–1245; b) Y. Abghoui, A. L. Garden, V. F. Hlynsson, S. Bjorgvinsdottir, H. Olafsdottir, E. Skulason, *Phys. Chem. Chem. Phys.* **2015**, *17*, 4909–4918.

[7] a) A. J. Haes, R. P. Van Duyne, *J. Am. Chem. Soc.* **2002**, *124*, 10596–10604; b) P. K. Jain, X. Huang, I. H. El-Sayed, M. A. El-Sayed, *Acc. Chem. Res.* **2008**, *41*, 1578–1586; c) S. K. Dondapati, T. K. Sau, C. Hrelescu, T. A. Klar, F. D. Stefani, J. Feldmann, *ACS Nano* **2010**, *4*, 6318–6322; d) K.-L. Lee, M.-J. Chih, X. Shi, K. Ueno, H. Misawa, P.-K. Wei, *Adv. Mater.* **2012**, *24*, OP253–OP259.

[8] a) Y. Tian, T. Tatsuma, *J. Am. Chem. Soc.* **2005**, *127*, 7632–7637; b) Y. Nishijima, K. Ueno, Y. Yokota, K. Murakoshi, H. Misawa, *J. Phys. Chem. Lett.* **2010**, *1*, 2031–2036; c) K. Ueno, H. Misawa, *NPG Asia Mater.* **2013**, *5*, e61.

[9] a) T. Hirakawa, P. V. Kamat, *J. Am. Chem. Soc.* **2005**, *127*, 3928–3934; b) P. Wang, B. Huang, X. Qin, X. Zhang, Y. Dai, J. Wei, M. H. Whangbo, *Angew. Chem. Int. Ed.* **2008**, *47*, 7931–7933; *Angew. Chem.* **2008**, *120*, 8049–8051; c) S. Linic, P. Christopher, D. B. Ingram, *Nat. Mater.* **2011**, *10*, 911–921.

[10] a) Y. Zhong, K. Ueno, Y. Mori, X. Shi, T. Oshikiri, K. Murakoshi, H. Inoue, H. Misawa, *Angew. Chem. Int. Ed.* **2014**, *53*, 10350–10354; *Angew. Chem.* **2014**, *126*, 10518–10522; b) Y. Zhong, K. Ueno, Y. Mori, T. Oshikiri, H. Misawa, *J. Phys. Chem. C* **2015**, *119*, 8889–8897.

[11] a) C. Reimann, T. Bredow, *J. Mol. Struct. THEOCHEM* **2009**, *903*, 89–99; b) O. Syzgantseva, M. Calatayud, C. Minot, *J. Phys. Chem. C* **2010**, *114*, 11918–11923; c) Y. Guo, S. Inoue, A. Kobayashi, J. Ohta, H. Fujioka, *Phys. Status Solidi RRL* **2013**, *7*, 207–210.

Received: December 3, 2015
Revised: January 27, 2016
Published online: February 17, 2016

